Physical Layer Performance Modeling of Modern Multicarrier Modulation Techniques

Waqar Anwar, Atul Kumar, Norman Franchi, *Member, IEEE*, and Gerhard Fettweis, *Fellow, IEEE*

***Abstract*— The fifth-generation (5G) and beyond standards are being challenged by the diverse requirements of modern use cases. Multicarrier modulation techniques are one of the key components of the physical layer (PHY) design, which has immense potential to improve efficiency and reliability. In current state-of-the-art wireless technologies (i.e., NR and IEEE 802.11ax) orthogonal frequency division multiplexing (OFDM) is used which has many disadvantages such as peak-to-average power ratio (PAPR), out-of-band emission (OOBE), and sensitivity to carrier frequency offset (CFO). To overcome these drawbacks several alternate multicarrier modulation techniques are being considered, such as discrete Fourier transform-spread-OFDM (DFT-s-OFDM), generalized frequency division multiplexing (GFDM), and orthogonal time-frequency space (OTFS). In this paper, we develop the physical layer abstraction (PLA) of these candidate multicarrier techniques to evaluate their performance under various use cases and scenarios. The PLA is a commonly used technique to avoid time-consuming PHY simulations in system-level simulators. To improve the accuracy of PLA in different fading conditions, we derive a fitting parameter as a function of the received signal-to-interference-plus-noise ratio (SINR) variance. The validation results show that performance can be accurately estimated through the proposed multicarrier PLA. Moreover, PLA techniques are at least thousands of times faster compared to PHY simulations.**

***Index Terms*— Physical layer abstraction, system-level simulation, link adaptation, multicarrier modulation techniques, eEESM, EESM, RBIR, OFDM, DFT-s-OFDM, GFDM, OTFS.**

I. Introduction

THE physical layer (PHY) of mobile communications systems is continuously evolving with each generation. Most recent standards of mobile communications such as Long-Term Evolution (LTE) and new radio (NR) uses orthogonal frequency division multiplexing (OFDM) as a multicarrier technique. Although OFDM is robust against the frequency-selectivity of the channel, it has many disadvantages such as out-of-band emission (OOBE), peak-to-average power ratio (PAPR), and sensitivity to carrier frequency offset (CFO). Another multicarrier technique currently being used for uplink transmission is discrete Fourier transform-spread-OFDM (DFT-s-OFDM) which addresses the issue of high PAPR. To reduce OOBE along with good PAPR performance the "generalized frequency division multiplexing (GFDM)" is recently proposed. However, the main problems of GFDM are the non-orthogonality generated by its prototype filters and sensitivity to CFO. In order to address all the above challenges and improve performance in time selective channels a new multicarrier modulation technique "orthogonal time frequency space (OTFS)" is proposed [2]. In OTFS symbols are localized in the delay-Doppler domain and the cyclic prefix (CP) protects orthogonality in both domains. Consequently, Doppler impairments can be mitigated and sensitivity to CFO could be reduced [3]. Among multicarrier techniques under consideration, the most suitable for enhanced vehicle-to-everything (eV2X) seems to be the OTFS.

To evaluate the performance of upcoming technologies in a range of fading scenarios, system-level simulations are generally used. In system-level evaluations, PHY simulations of each node become infeasible due to the huge processing required at PHY. Therefore, to speed up evaluations physical layer abstraction (PLA) is used which models PHY performance, e.g., packet error rate (PER) and throughput exclusively as a function of the received signal-to-interference-plus-noise ratio (SINR). However, the received symbols in a wideband multicarrier system could have variable channel gain due to the time-frequency selectivity of the channel. In this case, the instantaneous SINRs of received symbols are mapped to an effective SINR using PLA to obtain a single link quality indicator (LQI). After that the effective SINR could be used to predict PHY performance in the case of system-level simulations or to select optimal modulation and coding scheme (MCS) for link adaptation. Furthermore, the symbols received from different multicarrier techniques could have different SINR even under similar channel conditions which require multicarrier specific PLA modeling.

A. Related Work

In literature, exponential effective SINR mapping (EESM) [4], [5] and received bit information rate (RBIR) [6], [7] are the most commonly used effective SINR mapping algorithms. These algorithms are used to compute

Manuscript received August 26, 2021; revised January 2, 2022 and March 7, 2022; accepted April 7, 2022. Date of publication April 18, 2022; date of current version June 16, 2022. This work was supported in parts by the project "Industrial Radio Lab Germany" under contract 16KIS1010K, funded by the Federal Ministry of Education and Research (BMBF), Germany. An earlier version of this paper was presented in part at the IEEE Global Communication Conference (GLOBECOM), Waikoloa, Hawaii, USA, December 2019 [1] [DOI: 10.1109/GLOBECOM38437.2019.9014130]. The associate editor coordinating the review of this article and approving it for publication was J. Zhang. *(Corresponding author: Waqar Anwar.)*

Waqar Anwar and Gerhard Fettweis are with the Vodafone Chair Mobile Communications Systems, Department of Electrical Engineering, Technical University of Dresden, 01069 Dresden, Germany (e-mail: waqar.anwar@tu-dresden.de; gerhard.fettweis@tu-dresden.de).

Atul Kumar is with the Department of Electronics Engineering, IIT (BHU) Varanasi, Varanasi 221005, India (e-mail: atul.ece@iitbhu.ac.in).

Norman Franchi is with the Institute for Electrical Smart City Systems, Friedrich-Alexander-University (FAU) of Erlangen–Nuremberg, 91054 Erlangen, Germany (e-mail: norman.franchi@fau.de).

Color versions of one or more figures in this article are available at https://doi.org/10.1109/TCOMM.2022.3168084.

Digital Object Identifier 10.1109/TCOMM.2022.3168084

effective SINR of a received packet when symbols have variable SINR. Several studies have compared and evaluated their performance in system-level simulations and in link adaptation [5]–[10]. Results presented in these studies show that SINR mapping schemes can accurately predict PHY performance. However, their accuracy mainly depends on the channel profile and used MCS. Therefore, MCS and channel specific optimization is required. Recently in [11], a new effective SINR mapping algorithm named enhanced exponential effective SINR mapping (eEESM) is proposed which outperforms existing state-of-the-art (i.e., EESM and RBIR) algorithms. In this study, authors abstract the performance of different vehicle-to-everything (V2X) technologies and compare their performance in an Urban line-of-sight (LOS) V2X channel model. Further in [12], the eEESM is applied to multi-connectivity networks with link combining schemes. Nevertheless, the main focus of existing studies was to abstract the performance of OFDM system in frequency selective fading (FSF) channel.

In the context of future wireless technologies candidates, multicarrier techniques could be adopted to meet application-specific requirements. For example, in the case of eV2X doubly selective fading (DSF) will play a key role where new multicarrier techniques are expected to perform better, as analyzed in [13]. These multicarrier techniques could have different symbol SINRs even under similar fading conditions. As a result, the modeling of effective SINR of each multicarrier technique is required by taking into account the inter-carrier interference (ICI) effect and time-frequency selectivity of the channel. In this paper, we model these shortcomings by developing an enhanced PLA which accurately abstracts the characteristics of different multicarrier techniques under different fading conditions. We validate the developed PLA in each case by comparing its performance against PHY simulations. Lastly, we utilize PLA to evaluate the performance of multicarrier techniques in various fading channels. To the best of our knowledge, we are the first to propose a multicarrier-specific approach to abstract the PHY performance in both time and frequency selective channels.

B. Contribution

In this paper, we develop an enhanced PLA for modern multicarrier techniques (i.e., OFDM, DFT-s-OFDM, GFDM, and OTFS) to predict their performance under fading conditions. To abstract the performance, we derive the received SINR expressions for multicarrier techniques by taking into account the impact of ICI. Then the variable received SINRs in a packet due to fading are mapped to an effective SINR using eEESM. This takes into account the impact of channel selectivity on the symbols transmitted through these multicarrier techniques. To improve the mapping accuracy of eEESM in different fading conditions, the optimization of a fitting parameter is required. This optimization usually depends on multicarrier technique, MCS order, and channel selectivity. To reduce optimization complexity, we model the fitting parameter as a function of the mapping SINR variance which makes it independent of fading conditions. Therefore, the resultant effective SINR provides a more realistic performance evaluation in system-level simulations and enables reliable link adaptation. Furthermore, to verify the accuracy of PLA, PHY simulators of multicarrier techniques are implemented in MATLAB. The performance of proposed PLA modeling is quantified in terms of mean squared error (MSE) and compared with full PHY simulations. Subsequently, a comparison between PHY simulations and PLA is provided in terms of simulation time. In the end, applications of PLA are showcased by comparing the performance of multicarrier techniques under various fading conditions, e.g., FSF and DSF.

C. Organization

The paper is organized as follows. In Section II, an overview of multicarrier modulation techniques is provided and their pros and cons are discussed. In Section III, the ICI and its impact on communication performance is discussed. Afterward, the system model of multicarrier modulation techniques is described and SINR expressions are derived in Section IV. Further, in Section V, the eEESM based effective SINR mapping is explained, and its optimization against different fading conditions is discussed. In addition, the end-to-end multicarrier performance modeling using PLA under various fading conditions is presented. Subsequently, the performance of multicarrier PLA is evaluated against PHY simulations in Section VI, and error is quantified in terms of root-mean-square error (RMSE). Later in Section VII, the performance of multicarrier techniques is compared under various fading conditions using PLA. Finally, the main findings are summarized in Section VIII.

II. Overview of Multicarrier Techniques

Multicarrier modulations divide a broadband channel into closely spaced subcarriers for data transmissions. It offers multiple advantages over single carrier transmissions, which include resilience to narrowband fading and multipath effects. Furthermore, in the FSF channel each subcarrier experiences flat fading which can be equalized using single tap equalization. Therefore, multicarrier techniques are widely used in the current state-of-the-art wireless standards. The time-frequency domain representation of transmitted symbols using various multicarrier techniques is shown in Fig. 1. The K represents the frequency index and N/M represents the time domain index. Further explanation of their modulation principle and their pros and cons are discussed below.

A. Orthogonal Frequency Division Multiplex (OFDM)

OFDM divides a wideband channel into K parallel narrowband sub-channels such that each sub-channel can experience frequency flat behavior. The serial stream of transmitted symbols is converted into K parallel streams, which are then mapped to K orthogonal subcarriers. The advantage of dividing the channel is that a single tap equalization per subcarrier is possible. This reduces the complexity and increases the spectral efficiency of the system. Furthermore, a CP is appended with each OFDM symbol to mitigate inter-symbol interference (ISI) in multipath channels. It is currently

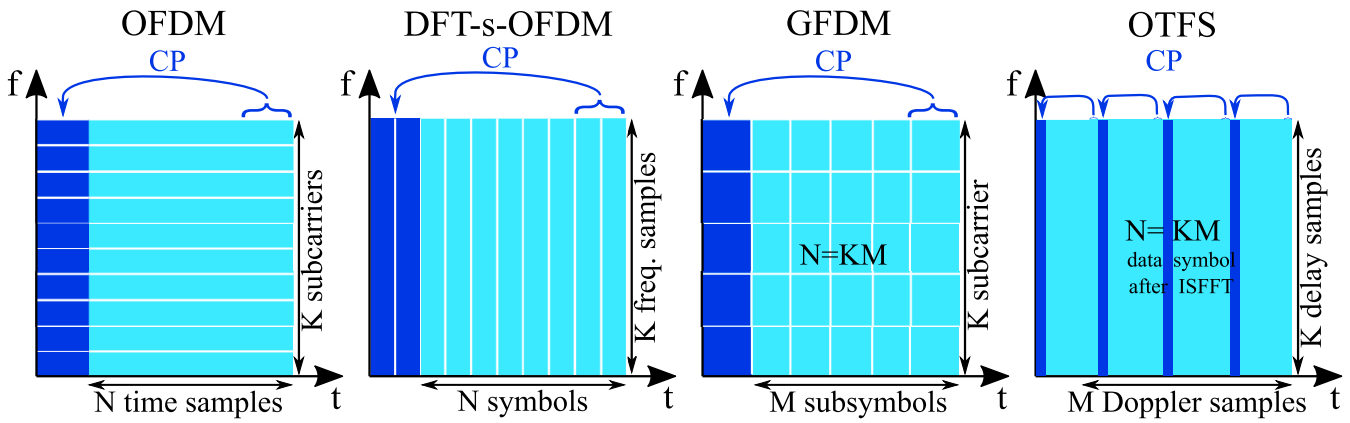

Fig. 1. Time-frequency representation of multicarrier modulation techniques.

being used by many wireless technologies, e.g., LTE, NR, and IEEE 802.11ac/ax. Its main advantages are easy equalization and low complexity [14], whereas disadvantages include high PAPR, OOBE, and sensitivity to CFO. In order to achieve better performance, many other multicarrier techniques have been proposed [2], [14].

B. DFT-Spread-OFDM (DFT-s-OFDM)

The DFT-s-OFDM, also known as single carrier frequency division multiplexing (SC-FDM), is similar to OFDM with an additional discrete Fourier transform (DFT) precoding that helps to reduce PAPR and improve the power efficiency of RF amplifiers. Therefore, it is suitable for low-budget devices and thus being used in LTE and NR for uplink transmissions. The transmitted symbols are first processed by M-point DFT, followed by resources mapping and N-point inverse DFT (IDFT) stage. It is important to mention here that M must be smaller than N, otherwise, for $M = N$ the cascaded DFT and IDFT processing would cancel each other. For this reason, the value of M is selected such that N becomes the multiple of M. There are two ways to map the M DFT samples to the subsequent N IDFT inputs: either localized or interleaved. More specifically, the output of DFT is either mapped to consecutive or uniformly spaced inputs of the OFDM modulator. Similar to OFDM, CP is used to avoid ISI and single tap equalization can be used after IDFT stage at the receiver. Disadvantages of DFT-s-OFDM are: increased complexity (compared to OFDM), OOBE, and sensitivity to CFO [14].

C. Generalized Frequency Division Multiplexing (GFDM)

The GFDM is another multicarrier modulation technique that uses a circular pulse shaping filter to reduce OOBE. The transmitted symbols are arranged into $K \times M$ blocks where K is the number of subcarriers and M is the number of subsymbols [14]. Afterward, a CP is appended to each GFDM block to maintain circularity and to ensure linear equalization at the receiver. The key step in GFDM modulation is the use of a digital pulse shaping filter at the transmitter and matched filter at the receiver. For that, the transmitted data is first up-sampled and then convolved with a pulse-shaping filter, e.g., a root-raised cosine function. Subsequently, the signal is match filtered at the receiver and down-sampled. Finally, an equalization in frequency domain (e.g. zero-forcing (ZF) and minimum mean squared error (MMSE)) can be used to recover the transmitted symbols [15]. The main benefit of GFDM is that using a special set of design parameters earlier introduced multicarrier techniques, i.e., OFDM, and DFT-s-OFDM can be generated. However, in the presence of Doppler or CFO the orthogonality gets lost which introduces ICI similar to previous techniques. To overcome ICI an iterative interference equalizer could be used however it significantly increases GFDM complexity [14].

D. Orthogonal Time Frequency Space (OTFS)

The OTFS is a newly proposed multicarrier technique that uses a different approach by interpreting channels in the delay-Doppler domain contrary to the traditionally used time-frequency domain. The fading channel can be characterized in the delay-Doppler domain by its delay taps τ and Doppler shifts ν, given as $h(\tau, \nu)$. Both channel representations are interrelated and conversion is possible using symplectic finite Fourier transform (SFFT). At the transmitter, symbols are arranged in the delay-Doppler grid and inverse SFFT (ISFFT) followed by Heisenberg transform is used to generate the time domain waveform. A Wigner Transformation and SFFT at the receiver could be used to convert symbols back into the delay-Doppler domain. Alternatively, it can also be implemented in the OFDM framework by precoding symbols using ISFFT before OFDM modulation at the transmitter and the associated SFFT after OFDM demodulation at the receiver [16]. In OTFS, symbols span the whole bandwidth in the frequency domain and the duration of a packet in the time domain. This enables OTFS to fully exploit the inherent time-frequency diversity of the channel. Moreover, a CP added in the time domain helps to maintain the orthogonality in the delay-Doppler domain, hence with a suitable equalizer, delay-Doppler interference can be nullified. Therefore, it is a favorable multicarrier technique for transmissions in high Doppler scenarios like eV2X communications. As it exploits time-frequency selectivity of the channel as an additional source of diversity instead of interference [16].

TABLE I

TIME SELECTIVITY (τ_s) AND ICI ($\sigma^2_{\nu_{\text{ICI}}}$) FOR VARIOUS COMBINATIONS OF DOPPLER SHIFT AND CARRIER SPACING

Carrier spacing / Doppler shift	15 kHz (LTE/ NR^0)		60 kHz (NR^2, $\approx$ 802.11ax)		156.25 kHz (802.11p/11bd)		312.5 kHz (802.11ac)	
	τ_s	$\sigma^2_{\nu_{\text{ICI}}}$	τ_s	$\sigma^2_{\nu_{\text{ICI}}}$	τ_s	$\sigma^2_{\nu_{\text{ICI}}}$	τ_s	$\sigma^2_{\nu_{\text{ICI}}}$
100 Hz	0.0067	-38.4 dB	0.0017	-50.5 dB	0.00064	-58.9 dB	0.00032	-64.9 dB
500 Hz	0.033	-24.5 dB	0.0083	-36.5 dB	0.0032	-44.9 dB	0.0016	-51.5 dB
1000 Hz	0.067	-18.4 dB	0.017	-30.5 dB	0.0064	-38.9 dB	0.0032	-45.5 dB
2000 Hz	0.13	-12.4 dB	0.033	-24.5 dB	0.013	-32.9 dB	0.0064	-38.9 dB

III. INTER-CARRIER INTERFERENCE

Multicarrier modulation techniques use CP to ensure the orthogonality of subcarriers under frequency dispersive channels. However, in eV2X communications, channels are time dispersive in nature due to Doppler shift [17], [18]. The Doppler shift cause interference among subcarriers in a multicarrier system, such as OFDM, also known as ICI. The impact of time dispersion could be determined by the product of maximum Doppler shift and symbol duration (inverse of subcarrier spacing). In other words, if the symbol duration is very large a smaller Doppler shift can also result in a reasonable ICI. Although, the used pulse shaping filter also plays a crucial role. In the case of OFDM, the variance of ICI at k-th subcarrier can be expressed (from [19]) as,

$$\sigma^2_{\nu}(k) = \sum_{n=1,n\neq k}^{K} |P(\frac{n-k}{T_{\text{s}}} + f_{\text{D}})|^2, \tag{1}$$

where T_{s} is the symbol duration, $P(\cdot)$ is the pulse shaping filter, K is the number of subcarriers, and f_D is the maximum Doppler shift. Many studies have investigated the impact of pulse shaping filters in reducing ICI power [19]–[22]. These studies show that the impact of ICI could be significantly reduced using advanced pulse shaping filters, e.g., raised cosine filter, improved sinc-power, and Nyquist-I. Nevertheless, the rectangular pulse shaping filter is currently being used by most state-of-the-art wireless technologies. The performance degradation due to Doppler can also be analyzed in terms of signal to interference ratio (SIR), given as

$$\text{SIR} = \frac{|P(f_{\text{D}})|^2}{\sum_{n=1,n\neq k}^{N} |P(\frac{n-k}{T_{\text{s}}} + f_{\text{D}})|^2}. \tag{2}$$

It can be observed from (1) that for a given pulse shaping filter, the ICI mainly depends on two factors, i.e., f_{D} and T_s. The ratio of these two factors can also be termed as time selectivity of the channel ($\tau_s = f_{\text{D}} \cdot T_s$). In Fig. 2, values of ICI (on the left side) and SIR (on the right side) are plotted as a function of τ_s for the case of rectangular pulse shaping filter.

Results show that with the increase in ratio from 0.02 to 0.2 the ICI power increases by $\approx$20dB, hence SIR reduces from 28 dB to 8 dB. These results demonstrate that in the case of a higher τ_s system becomes ICI denominated and performance could not be improved by increasing the transmit power. Furthermore, the ICI variance for various combinations of carrier spacing and Doppler shift is provided in Table I.

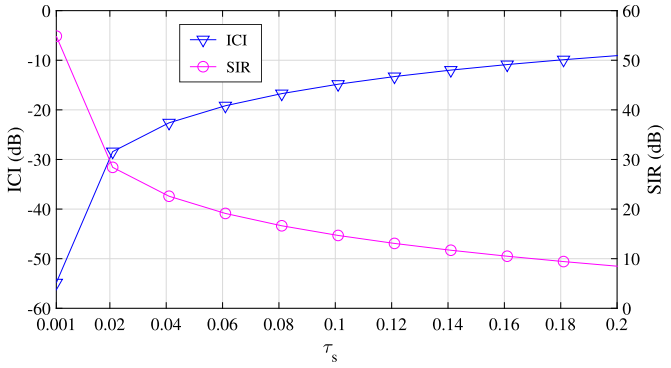

Fig. 2. ICI and SIR value for various values of τ_s.

The choice of carrier spacing plays an important role to improve performance in high Doppler scenarios. For example, the LTE-V2X could become ICI dominated even at 500 Hz, whereas using 60kHz carrier spacing (defined by NR with $u = 2$) SIR can be improved by $\approx$12dB. Similarly, due to lower carrier spacing used by IEEE 802.11p/bd, 20dB higher SIR compared to LTE/ NR^0 can be achieved. Although the increase in carrier spacing can reduce ICI, it negatively affects the robustness against frequency dispersion. This is due to the decrease in symbol duration and consequently the CP. Therefore, it must be considered while selecting an optimal carrier spacing. Finally, it is important to mention that the ICI can also be minimized using iterative interference cancellation schemes [23]–[26].

IV. SYSTEM MODEL

The multicarrier modulation system model is illustrated in Fig. 3. At the transmitter, the data packet **D** is first encoded using low-density parity check (LDPC) codes (as defined by NR) then M-QAM constellations mapping is performed. The resulting symbols are further processed by multicarrier-specific modulators and a time domain signal $s(t)$ is generated. The transmitted signal is then convolved with a multipath channel denoted as $h_t(\tau)$ and additive white Gaussian noise (AWGN) noise is added. At the receiver, the signal is demodulated, and channel estimation and equalization are performed. Following assumptions are made to simplify modeling: perfect synchronization is possible in time-frequency and error-free channel estimation is available at the receiver. In the later part of this section, the step-by-step processing of each multicarrier

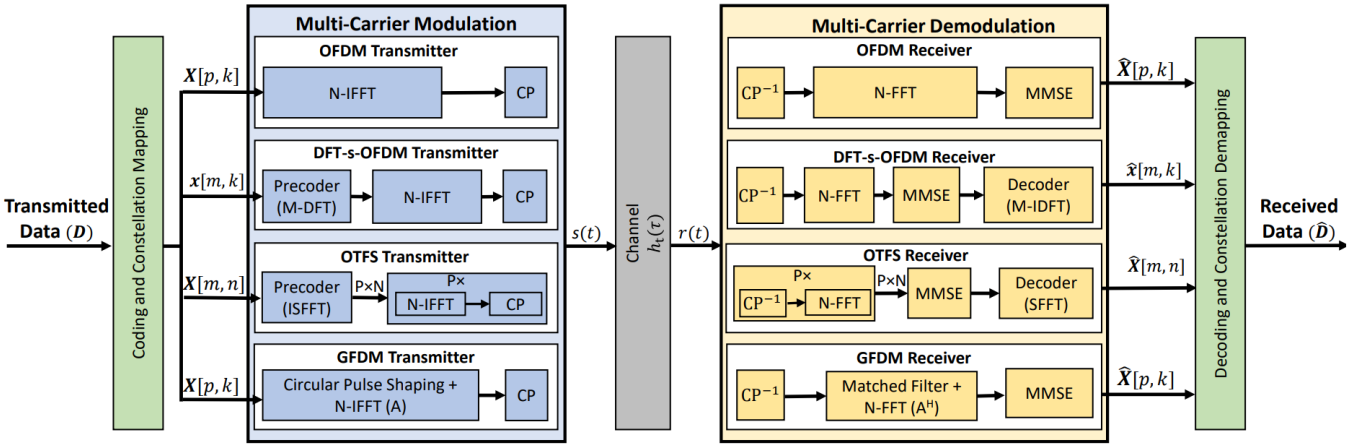

Fig. 3. Multicarrier modulation and demodulation system model.

technique is discussed and the received SINR expressions are derived.

A. Symbols and Notations

The frequency domain matrix is denoted with a capital bold symbol, the time domain matrix is denoted by a small bold symbol, the frequency domain signal is denoted by a capital symbol, the time domain signal is denoted by a small symbol, the transpose operator is denoted by $(\cdot)^T$, the Hermitian operation is denoted by $(\cdot)^H$, and identity matrix is denoted by $\mathbf{I}$.

B. OFDM

The data packet ($\mathbf{D}$) after encoding and constellation mapping could be represented by a matrix $\mathbf{X}$ of $M \times K$ dimensions, where M is the number of OFDM symbols and K is the number of data subcarriers. The time duration of an OFDM symbol is T_s, where subcarrier spacing is equal to $\frac{1}{T_s}$. The modulated symbols $\mathbf{X}$ inside a packet could be expressed as

$$\mathbf{X} = [\mathbf{X}(1), \mathbf{X}(2), \ldots, \mathbf{X}(M)], \tag{3}$$

here

$$\mathbf{X}(m) = [X(m,1), X(m,2), \ldots, X(m,K)]^T \tag{4}$$

whereas $X(m,k)$ denotes the symbol mapped on k-th subcarrier of m-th OFDM symbol. The symbols mapped on the m-th OFDM symbol $\mathbf{X}(m) = [X(1), X(2), \ldots, X(K)]^T$ are processed by IDFT stage to generate a time domain signal represented as

$$\mathbf{s} = \mathbf{F}^H I_N \mathbf{X}, \tag{5}$$

here $\mathbf{F}^H \in \mathbb{C}^{N \times N}$ is the IDFT matrix, and I_N is the identity matrix which maps the symbols to available data subcarriers. Subsequently, a CP is added to avoid ISI, then the modified signal ($\tilde{\mathbf{s}}$) of sample length $\tilde{N}$ is convoluted with a multipath channel, and noise is added. As mentioned earlier, it is assumed that the CP duration is greater than the maximum excess delay of the channel, therefore no ISI cancellation scheme is needed. The received signal ($\tilde{\mathbf{r}}$) can be written as

$$\tilde{\mathbf{r}} = \tilde{\mathbf{s}} * \mathbf{h} + \boldsymbol{\rho} \tag{6}$$

where $*$ is the linear convolution operation and $\boldsymbol{\rho}$ is AWGN noise with zero mean and variance σ_ρ^2. At the receiver, first CP is detached then the signal is converted to the frequency domain using the DFT stage. The symbols received at k-th subcarrier and m-th OFDM symbol can be represented as

$$Y(m,k) = \underbrace{H(m,k)X(m,k)}_{\text{desired signal}} + \underbrace{\sum_{n=1, n\neq k}^{N} H(m,n)X(m,n)}_{\nu_{\text{ICI}}(m,k)} + \underbrace{\rho(m,k)}_{\text{noise}} \tag{7}$$

where $H(m,k)$ denote the channel gain at k-th subcarrier of m-th OFDM symbol and $\rho(m,k)$ is the AWGN noise with variance σ_ρ^2. The Doppler induced ICI observed on multipath components is represented as $\nu_{\text{ICI}}(m,k)$. Finally, the symbols are equalized using MMSE equalizer. The recovered symbol on the k-th subcarrier of m-th OFDM symbol can be represented as

$$\hat{X}(m,k) = W(m,k)H(m,k)X(m,k) + W(m,k)\left(\nu_{\text{ICI}}(m,k) + \rho(m,k)\right) \tag{8}$$

whereas $W(m,k)$ represents the MMSE equalizer matrix defined as

$$W(m,k) = \left(\frac{\sigma_{\rho+\nu}^2}{\sigma_x^2} + H(m,k)^* H(m,k)\right)^{-1} H(m,k)^*, \tag{9}$$

whereas $\sigma_{\rho+\nu}^2$ is the thermal noise plus ICI variance and σ_x^2 is the transmitted symbol variance. The noise and ICI powers are assumed equally distributed on all subcarriers and subsymbols. After equalization, the received symbol variance can be written as

$$\sigma_{\hat{\mathbf{x}}}^2(m,k) = \left(\frac{|H(m,k)|^2}{|H(m,k)|^2 + \frac{\sigma_{\rho+\nu}^2}{\sigma_x^2}}\right)^2 \sigma_x^2 = \alpha_{\text{MMSE}}(m,k)\sigma_x^2, \tag{10}$$

where α_{MMSE} is the signal enhancement due to MMSE equalization. Similarly, noise and interference will be enhanced as

$$\sigma_{\rho}^2(m,k) = \left(\frac{|H(m,k)|}{|H(m,k)|^2 + \frac{\sigma_{\rho+\nu}^2}{\sigma_x^2}}\right)^2 \sigma_{\rho+\nu}^2 = \beta_{\text{MMSE}}(m,k)\sigma_{\rho+\nu}^2, \tag{11}$$

where β_{MMSE} is the noise and interference enhancement factor due to MMSE equalization. Now, the SINR at k-th subcarrier of the m-th OFDM symbol can be expressed as

$$\gamma(m,k) = \frac{\sigma_{\hat{\text{x}}}^2(m,k)}{\sigma_{\rho}^2(m,k)} = \frac{\alpha_{\text{MMSE}}(m,k)\,\sigma_x^2}{\beta_{\text{MMSE}}(m,k)\sigma_{\rho+\nu}^2},$$

$$\gamma(m,k) = \frac{\left(\frac{|H(m,k)|^2}{|H(m,k)|^2+\frac{\sigma_{\rho+\nu}^2}{\sigma_x^2}}\right)^2 \sigma_x^2}{\left(\frac{|H(m,k)|}{|H(m,k)|^2+\frac{\sigma_{\rho+\nu}^2}{\sigma_x^2}}\right)^2 \sigma_{\rho+\nu}^2} = |H(m,k)|^2 \frac{\sigma_x^2}{\sigma_{\rho+\nu}^2}. \tag{12}$$

The ICI power (σ_ν^2) at k-th subcarrier can be estimated using (1). It could be safely assumed that σ_ν^2 is constant over all subcarriers as Doppler does not significantly vary in 10 MHz bandwidth. The signal attenuation due to Doppler induced CFO can be accounted as P(f_{D}).

C. DFT-s-OFDM

The data packet in DFT-s-OFDM can be arranged in time domain matrix $\mathbf{x}$ with $M \times P$ dimensions, where M is the size of the DFT matrix and P is the number of DFT-s-OFDM symbols, given as

$$\mathbf{x} = [\mathbf{x}(1), \mathbf{x}(2), \ldots, \mathbf{x}(P)], \tag{13}$$

where

$$\mathbf{x}(p) = [x(p,1), x(p,2), \ldots, x(p,M)]^T. \tag{14}$$

The modulated symbols at each p-th columns are passed through DFT precoding stage leading to $\mathbf{X} = \mathbf{F}_M\mathbf{x}$, here $\mathbf{F}_M \in \mathbb{C}^{M\times M}$ denote the DFT operation. Afterward, samples are mapped to orthogonal subcarriers by means of a resource mapper $\mathbf{I}_{N_m}$ which maps M frequency samples to N_m allocated subcarriers from a set of N subcarriers followed by IDFT operation $\mathbf{F}_N^H$. In this paper, M equal to 16 is used such that each DFT sample is uniformly mapped to every fourth subcarrier also called interleaving. The resulting data samples can be expressed as

$$\mathbf{s} = \mathbf{F}_N^H \mathbf{I}_{N_m}\mathbf{X}. \tag{15}$$

Now, the CP is inserted at the end of each DFT-s-OFDM symbol to avoid ISI. The resulting signal ($\tilde{\mathbf{s}}$) convolved with the channel impulse response and noise is added. The earlier made assumptions regarding CP duration, equalization, and CFO for OFDM are also valid for the case of DFT-s-OFDM. At the receiver end, first CP is detached, then DFT operation is performed, and received samples are equalized in the frequency domain. The received samples at the p-th DFT-s-OFDM symbol are expressed as

$$\mathbf{Y} = \mathbf{H}\mathbf{I}_{N_m}\mathbf{X} + \boldsymbol{\nu}_{\text{ICI}} + \boldsymbol{\rho}, \tag{16}$$

where $\mathbf{H} = [H(1), H(2), \ldots, H(N_m)]$ denote the channel response at each subcarrier, $\boldsymbol{\nu}_{\text{ICI}} = [\nu_{\text{ICI}}(1), \nu_{\text{ICI}}(2), \ldots, \nu_{\text{ICI}}(N_m)]$ is the ICI at each subcarrier due to Doppler and $\boldsymbol{\rho}$ denote the AWGN noise. The ICI variance at k-th subcarrier can be calculated as

$$\nu_{\text{ICI}}(k) = \sum_{n=1, n\neq k}^{N} H(n)X(n). \tag{17}$$

In the next step, samples are demapped and converted into time domain symbols using the IDFT operation. The recovered symbols from a DFT-s-OFDM symbol are represented as

$$\hat{\mathbf{x}} = \mathbf{F}_M^H\mathbf{W}\mathbf{H}\mathbf{I}_{N_m}\mathbf{X} + \mathbf{F}_M^H\mathbf{W}(\boldsymbol{\nu}_{\text{ICI}} + \boldsymbol{\rho}), \tag{18}$$

whereas $\mathbf{W}$ is the MMSE equalization matrix, given as

$$\mathbf{W} = \left(\frac{\sigma_{\rho+\nu}^2}{\sigma_x^2}\boldsymbol{I}_{N_m} + \mathbf{H}^H\mathbf{H}\right)^{-1}\mathbf{H}^H, \tag{19}$$

whereas $\sigma_{\rho+\nu}^2$ is the noise plus interference variance and σ_x^2 is the signal power. The desired signal power of m-th data symbol received at p-th DFT-s-OFDM symbol is

$$\sigma_{\hat{\text{x}}}^2(p,m) = \left(\frac{1}{N_m}\sum_{k=1}^{N_m}\frac{|H(p,k)|^2}{|H(p,k)|^2+\frac{\sigma_{\rho+\nu}^2}{\sigma_x^2}}\right)^2 \sigma_x^2 = \sigma_{\text{MMSE}}(p,m)\,\sigma_x^2, \tag{20}$$

where N_m are the index of data subcarriers over which m-th symbol is spread and σ_{MMSE} is the desired signal amplification factor. It can be noticed that the signal power is independent of index m as all data symbols spread over N_m subcarriers will have the same amplification factor. The earlier made assumptions for OFDM regarding noise and ICI are also valid for DFT-s-OFDM. As a result, the noise and ICI amplification from (18) can be obtained as

$$\sigma_{\rho}^2(p,m) = \frac{1}{N}\sum_{k=1}^{N}\left(\frac{|H(p,k)|}{|H(p,k)|^2+\frac{\sigma_{\rho+\nu}^2}{\sigma_x^2}}\right)^2 \sigma_{\rho+\nu}^2 = \beta_{\text{MMSE}}(p,m)\sigma_{\rho+\nu}^2. \tag{21}$$

In addition to noise and ICI, the MMSE equalizer accumulate self-interference which can be represented as for m-th received symbol

$$\sigma_{\text{I}}^2(p,m) = \left(\sum_{l=1,l\neq m}^{M}\sigma_{\hat{\text{x}}}^2(p,l)\right), = \frac{\sigma_x^2}{N_m}\sum_{k=1}^{N_m}\left(\frac{|H(p,k)|^2}{|H(p,k)|^2+\frac{\sigma_{\rho+\nu}^2}{\sigma_x^2}}\right)^2 - \sigma_{\text{MMSE}}(p,m)\sigma_x^2. \tag{22}$$

where M denotes the number of received symbols in each DFT-s-OFDM symbol. The addition and simplification of all interference terms lead to

$$\begin{aligned}&\sigma_\rho^2(p,m)+\sigma_{\mathrm{I}}^2(p,m)\\&=\frac{\sigma_x^2}{N}\sum_{k=1}^{N}\left(\frac{|H(p,k)|^2\left(\frac{\sigma_{\rho+\nu}^2}{\sigma_x^2}+|H(p,k)|^2\right)}{\left(|H(p,k)|^2+\frac{\sigma_{\rho+\nu}^2}{\sigma_x^2}\right)^2}\right)\\&\quad-\sigma_{\mathrm{MMSE}}(p,m)\sigma_x^2,\\&=\sigma_x^2(\sqrt{\sigma_{\mathrm{MMSE}}(p,m)}-\sigma_{\mathrm{MMSE}}(p,m)).\end{aligned}\tag{23}$$

Finally, the SINR of m-th symbol received at p-th DFT-s-OFDM symbol can be obtained as

$$\begin{aligned}\gamma(p,m)&=\frac{\alpha_{\mathrm{MMSE}}(p,m)\sigma_x^2}{\sigma_\rho^2(p,m)+\sigma_{\mathrm{I}}^2(p,m)}\\&=\frac{1}{(1/\sqrt{\alpha_{\mathrm{MMSE}}(p,m)})-1}.\end{aligned}\tag{24}$$

If an ideal interference cancellation scheme is used the SINR can be written as

$$\gamma(p,m)=\frac{\alpha_{\mathrm{MMSE}}(p,m)\sigma_x^2}{\beta_{\mathrm{MMSE}}(p,m)\sigma_{\rho+\nu}^2}.\tag{25}$$

D. GFDM

In the case of GFDM, the data packet is arranged as a matrix ($\mathbf{X}$) of size $N\times P$, here $N=MK$, where K denotes the number of subcarriers, on each subcarrier M symbols are mapped, and P is the number of total symbols in a GFDM block, given as

$$\mathbf{X}=[\mathbf{X}(1),\mathbf{X}(2),\ldots,\mathbf{X}(P)],\tag{26}$$

where

$$\mathbf{X}(p)=[x(p,1),x(p,1),\ldots,x(p,N)]^T.\tag{27}$$

Symbols at p-th column are processed by a circular pulse-shaping filter written as

$$g_{k,m}[n]=g[(n-mK)\bmod N]\,e^{\frac{-\mathrm{j}2\pi\mathrm{kn}}{K}},\tag{28}$$

whereas $g[n]$ denote the prototype filter, e.g., raised cosine in our case, $\bmod N$ denote the modulo N operation which produces circularly shifted symbols in time and exponential part produce shifted symbols in frequency. The resulting signal is represented as

$$\mathbf{s}=\mathbf{A}\boldsymbol{I}_{MK,M}\mathbf{X},\tag{29}$$

where $I_{MK,M}$ is the resource mapper, and $\mathbf{A}=\left[\boldsymbol{g}_{0,0}\cdots\boldsymbol{g}_{K-1,0},\cdots,\boldsymbol{g}_{0,M-1}\cdots\boldsymbol{g}_{K-1,M-1}\right]\in\mathbb{C}^{MK\times MK}$. After adding the CP to each GFDM block, the resulting signal ($\tilde{\mathbf{s}}$) passes from the multipath channel and AWGN noise is added. On the receiver, inverse processing is carried out, which includes CP removal and match filtering. The received symbols in each GFDM block can be expressed as

$$\mathbf{Y}=\mathbf{HA}\boldsymbol{I}_{MK,M}\mathbf{X}+\boldsymbol{\nu}_{\mathrm{ICI}}+\boldsymbol{\rho},\tag{30}$$

where $\mathbf{H}$ is the channel matrix with $MK\times MK$ entries, $\boldsymbol{\nu}_{\mathrm{ICI}}$ is the ICI and $\boldsymbol{\rho}$ is the noise. Now, the equalized symbols can be given as

$$\hat{\mathbf{X}}=\mathbf{WHA}\boldsymbol{I}_{MK,M}\mathbf{X}+\mathbf{AW}(\boldsymbol{\nu}_{\mathrm{ICI}}+\boldsymbol{\rho}),\tag{31}$$

whereas $\mathbf{W}$ is the equalization matrix of $MK\times MK$ dimensions written as

$$\mathbf{W}=\left(\frac{\sigma_{\rho+\nu}^2}{\sigma_x^2}\boldsymbol{I}_{MK,MK}+(\mathbf{HA})^H(\mathbf{HA})\right)^{-1}(\mathbf{HA})^H.\tag{32}$$

After following similar steps as used to drive SINR for DFT-s-OFDM, the post-equalization SINR of n-th data symbol at p-th GFDM symbol is given as

$$\gamma(p,n)=\frac{1}{(1/\sqrt{\alpha_{\mathrm{MMSE}}(p,n)})-1},\tag{33}$$

where $\alpha_{\mathrm{MMSE}}(p,n)$ given as

$$\alpha_{\mathrm{MMSE}}(p,n)=\left(\frac{1}{MN}\sum_{m=1}^{M}\sum_{n=1}^{N}\frac{(\mathbf{HA})^2}{(\mathbf{HA})^2+\frac{\sigma_{\rho+\nu}^2}{\sigma_x^2}}\right)^2.\tag{34}$$

In the case of ideal interference cancellation scheme is used the SINR can be obtained similar to (25).

E. OTFS

The modulated data packet $\mathbf{X}$ is arranged in the delay-Doppler domain as a matrix of $N\times M$ symbols. These symbols are converted into time-frequency domain samples using ISFFT (S^H) precoding. The SFFT is equivalent to IFFT operation in the Doppler domain with size $M\times M$ and FFT in the delay domain with size $N\times N$ [16]. The resulting SFFT precoded samples are then processed by the OFDM modulator and demodulator. As the number of precoded samples is higher than the maximum number of OFDM subcarriers, therefore multiple OFDM symbols are required to transmit the packet. After IDFT operation $\mathbf{F}_N^H$, the time domain signal can be expressed as

$$\mathbf{s}=\mathbf{F}_N^H\mathbf{S}^H\mathbf{X}\tag{35}$$

The transmitted waveform is further processed in a similar manner as mentioned earlier for other multicarrier techniques. As the packet is transmitted using multiple OFDM symbols and equalization is performed in the time-frequency domain, multiple CPs (one per each OFDM symbol) are used in the time-frequency domain. The received symbols after performing SFFT and equalization can be written as

$$\hat{\boldsymbol{X}}=\mathbf{SWHS}^H\mathbf{X}+\mathbf{SW}(\boldsymbol{\nu}_{\mathrm{ICI}}+\boldsymbol{\rho}),\tag{36}$$

whereas $\mathbf{W}$ represent MMSE equalization matrix of $M\times N$ dimensions written as

$$\mathbf{W}=\left(\frac{\sigma_{\rho+\nu}^2}{\sigma_x^2}\boldsymbol{I}_{M,M}+\mathbf{H}^H\mathbf{H}\right)^{-1}\mathbf{H}^H,\tag{37}$$

where $\mathbf{H}$ is the channel response matrix of $N\times M$ dimensions. The received SINR of symbols can be obtained as

$$\gamma=\frac{1}{(1/\sqrt{\alpha_{\mathrm{MMSE}}})-1},\tag{38}$$

TABLE II
OPTIMIZED VALUE OF β (β_{OPT}) FOR DIFFERENT MULTICARRIER TECHNIQUES

MCS	OFDM	DFT-s-OFDM	GFDM	OTFS
1/2 QPSK	-0.004$\sigma_{\bar{\gamma}}$+1.86	-0.016$\sigma_{\bar{\gamma}}$+1.80	-0.018$\sigma_{\bar{\gamma}}$+1.78	1.88
1/2 16-QAM	-0.12$\sigma_{\bar{\gamma}}$+8.9	-0.14$\sigma_{\bar{\gamma}}$+8.8	-0.15$\sigma_{\bar{\gamma}}$+8.6	9.2
3/4 16-QAM	-0.15$\sigma_{\bar{\gamma}}$+9.2	-0.18$\sigma_{\bar{\gamma}}$+8.9	-0.19$\sigma_{\bar{\gamma}}$+8.7	9.4
3/4 64-QAM	-0.84$\sigma_{\bar{\gamma}}$+ 38.4	-0.92$\sigma_{\bar{\gamma}}$+36.8	-0.92$\sigma_{\bar{\gamma}}$+36.0	38.4

whereas α_{MMSE} is defined as

$$\alpha_{\text{MMSE}} = \left(\frac{1}{MN} \sum_{m=1}^{M} \sum_{n=1}^{N} \frac{|H(m,n)|^2}{|H(m,n)|^2 + \frac{\sigma_{\rho+\nu}^2}{\sigma_x^2}} \right)^2 . \quad (39)$$

The time domain CP in OTFS protect symbols from both delay and Doppler impairments, if the duration in the delay domain is lager than the maximum delay spread and in Doppler domain is larger than the Doppler shift. Interference free SINR can be obtained similar to (25), if ideal interference cancellation scheme is used.

V. PHYSICAL LAYER ABSTRACTION FOR MULTICARRIER TECHNIQUES

In general, PLA is used to estimate link performance as a function of the received SINR. However, the current wireless technologies use various channel coding schemes which do not have a closed-form expression for symbol error rate (SER) or PER. In addition, if the channel is time or frequency selective the received symbols inside a packet could have variable SINRs. In this case, PER depends on the average SER given as

$$P_{\text{eff}} = \frac{1}{N} \sum_{n=1}^{N} P_n \,, \quad (40)$$

where N denote the number of total received symbols in a packet and P_n is the SER of n-th received symbol. For the case of BPSK, effective SINR (γ_{eff}) from (40) can be rewritten as

$$Q\left(\sqrt{2\gamma_{\text{eff}}}\right) = \frac{1}{N} \sum_{n=1}^{N} Q\left(\sqrt{2\gamma_{\text{n}}}\right), \quad (41)$$

here γ_{n} denote the SINR of n-th received symbol, which could be obtained using multicarrier specific SINR expressions derived in Section IV. By observing (41), it can be said that $\gamma_{\text{eff}} \neq \frac{1}{N}\sum_{n=1}^{N} \gamma_n$, therefore average received SINR cannot be used to predict the average SER. Consequently, effective SINR mapping techniques are used to derive an AWGN equivalent SNR also known as effective SINR, details are provided in Appendix VIII. The performance of a fading channel at a given effective SINR is equivalent to the AWGN channel. This equivalence allows the reusing of SNR vs. PER lookup tables generated under the AWGN assumption to estimate performance in a range of fading conditions. According to [11], the newly proposed eEESM mapping technique outperforms EESM and RBIR, hence will be used in this paper. It is derived by upper bounding the SER by using a tighter upper bound on error function, given by $Q(x) \approx \frac{1}{\sqrt{2\pi(x^2+1)}} \exp\left(-\frac{x^2}{2}\right)$ [27, eq. (21)]. By using this bound, SER for BPSK [28, eq. (5.101)] can be written as

$$P_n \approx \frac{1}{\sqrt{2\pi(2\gamma+1)}} \exp(-\gamma) \,. \quad (42)$$

Now, for N received symbols (42) could be rewritten as

$$\begin{aligned} P_{\text{eff}} &\approx \frac{1}{\sqrt{2\gamma_{\text{eff}}+1}} \exp(-\gamma_{\text{eff}}) \\ &= \frac{1}{N} \sum_{n=1}^{N} \frac{1}{\sqrt{2\gamma_n+1}} \exp(-\gamma_n) \,. \end{aligned} \quad (43)$$

Solving for the effective SINR leads to the following generic expression

$$\gamma_{\text{eff}} = \frac{\beta}{2} \left\{ \mathcal{W}\left[\exp(1) \left(\frac{1}{N} \sum_{n=1}^{N} \frac{1}{\sqrt{\frac{2\gamma_n}{\beta}+1}} \exp\left(-\frac{\gamma_n}{\beta}\right) \right)^{-2} \right] - 1 \right\}. \quad (44)$$

whereas $\mathcal{W}(\cdot)$ denote the Lambert-W function given as $\mathcal{W}(xe^x) = x$ [29] and β is the modulation and channel dependent parameter. The default values of β for various modulations are as follows: 1, 2, 10, 42, and 170 for BPSK, QPSK, 16-QAM, 64-QAM, and 256-QAM, respectively. These values are obtained from SER expression of these modulation schemes [11]. The optimum value of β is obtained by using the least square fit among PER points in a fading channel such that the MSE can be minimized in reference to AWGN PER. Thus, it can be expressed as

$$\beta_{\text{opt}} = \arg\min_{\beta} \left| \gamma_{\text{AWGN}} - \gamma_{\text{eff}}(\beta) \right|^2 . \quad (45)$$

The traditional β optimization depends on the MCS and channel profile. Therefore, it needs to be tuned for each multicarrier technique, MCS, and channel profile. Now, if the PLA is required to be applied for a range of channel conditions with various power delay profile (PDP)s and fading distributions, either a default value of β could be used with the suboptimal performance or optimization should be carried out for all possible cases. Consequently, the optimization of β becomes infeasible due to complexity.

To reduce optimization complexity, we model β as a function of the received SINR variance. As variance directly depends on the channel conditions which in turn require optimization of β to improve accuracy. Therefore, we obtain the dependency of β_{opt} on the variance through PHY simulations

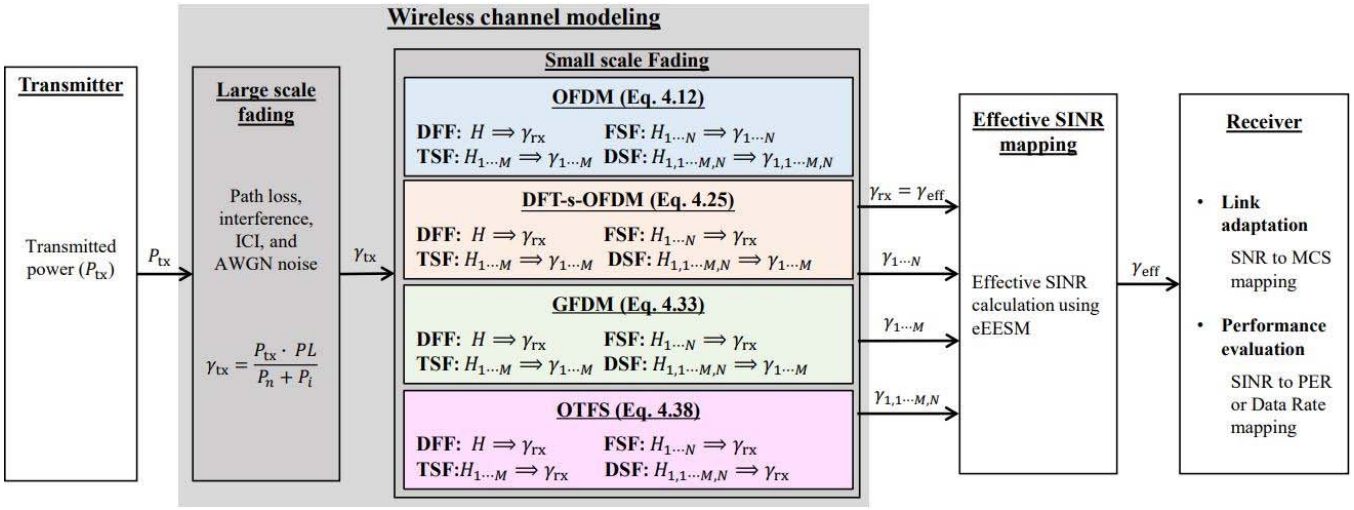

Fig. 4. PLA modeling for multicarrier modulation techniques.

and use linear regression to extend it for the general case, given as

$$\beta = a \cdot \sigma_{\bar{\gamma}} + b \tag{46}$$

where a is the slope of the curve, $\sigma_{\bar{\gamma}}$ is the variance of the received SINR vector $\bar{\gamma}$ being mapped to an effective SINR and b is constant. After obtaining the variables a and b from a few channel realizations, β can be easily generalized to other fading conditions. Moreover, this approach provides optimized β along each SINR point of PER curve, contrary to the approach used for EESM and RBIR in literature [5], [7], where one value of β is used to fit all SINR points along the PER curve. In Table II optimized value of β are provided for different MCSs and multicarrier techniques. In the case of OTFS, β only depends on b due to the fact that the received symbols in one OTFS block have equal SINR, in other words, their variance is zero.

The concept of modeling end-to-end PHY performance of considered multicarrier techniques using PLA is illustrated in Fig. 4. Depending on the channel selectivity symbol SINRs are estimated using the SINR expressions derived in the previous section for different multicarrier techniques. If multiple SINRs are expected, effective SINR is calculated using (44) and performance is predicted using pre-computed AWGN lookup tables.

In the case of OFDM, each data symbol is mapped to a unique subcarrier for the duration of T_s. Therefore, under frequency or time selective fading symbols could experience variable channel gain. If the channel is selective, its gain could be either represented with a vector, as in the case of FSF or time selective fading (TSF), or with a matrix, as in the case of DSF. Consequently, the received packet has multiple SINRs, which should be mapped to an effective SINR using (44). On the other hand, if the channel is doubly flat fading (DFF), effective SINR mapping is not required, since all symbols inside a packet will have equal SINR. As a result, the channel is represented with a single gain, and the received SINR obtained using (12) will serve as an effective SINR. Contrary to OFDM, data symbols in DFT-s-OFDM are spread over the frequency domain. If received symbols inside a packet are mapped at the same subcarriers indexes then effective SINR computation is not needed for FSF channel, as all received symbols will have equal SINR. However, if data symbols are transmitted over different groups of subcarriers while mapping M DFT samples to N available subcarriers (N/M groups can be made), effective SINR will be calculated among these groups. Nevertheless, for the case of DSF channel SINR mapping is required among DFT-s-OFDM symbol blocks for which channel is not considerably flat. For the other two cases, i.e., DFF and TSF, effective SINR mapping is similar to OFDM. In GFDM, the N data symbols are spread over K subcarrier and M subsymbols. Therefore, under FSF or DFF channel SINR mapping is not required, similar to DFT-s-OFDM. Contrarily, under DSF or TSF fading SINR mapping could be required among GFDM blocks, depending on the relation between coherence time and packet duration. The data packet in OTFS is commonly transmitted in one transversal block, which means data symbols are equally spread over time and frequency. In this case, no SINR mapping is required and the received SINR is used for performance evaluation. However, if data is transmitted over multiple transversal blocks then effective SINR mapping would be required among these blocks.

VI. Evaluation of Multicarrier PLA

In this section, multicarrier modulation-specific PHY simulators are used to validate the accuracy of developed PLA. On one hand, PER is calculated using a complete PHY chain, on the other hand, performance is predicted using the multicarrier-specific PLA. The fading channel between users is modeled either as FSF or DSF using the PDP given in Table III. The ideal channel estimation and CFO correction are assumed. Other relevant parameters for simulations are available in Table III. The PLA validation is carried out here in two steps: accuracy of effective SINR mapping in reference to performance in AWGN channel, and PLA prediction accuracy compared to PHY simulations in a fading channel.

TABLE III
SIMULATION PARAMETERS

Parameter	Value
PHY settings	
Channel bandwidth	10 MHz
FFT length	64 (others), 16 for GFDM (K = 16, M = 4)
Carrier Spacing	156.25 KHz (others), 625 KHz (GFDM)
Symbol duration	6.4 μs
Cyclic prefix	1.6 μs
Payload size (P_b)	300 bytes
Modulation and coding schemes (MCS)	given in Table II
Channel coding	LDPC (fifth generation (5G) NR)
Packet duration (T_p) for considered MCSs	[304, 152, 104, 72]µs
Channel equalization method	MMSE
Small scale fading	
Maximum doppler shift (f_m)	100 Hz (FSF) / 2000 Hz (DSF)
Relative power of each tap	[0 -10 -14 -18] dB
Excess delay of each tap	[0 0.4 0.7 1] µs
Coherence time (50%)	4.23 ms (FSF), 0.21 ms (DSF)
Coherence bandwidth (50%)	≈1 MHz
Fading distribution	Rayleigh

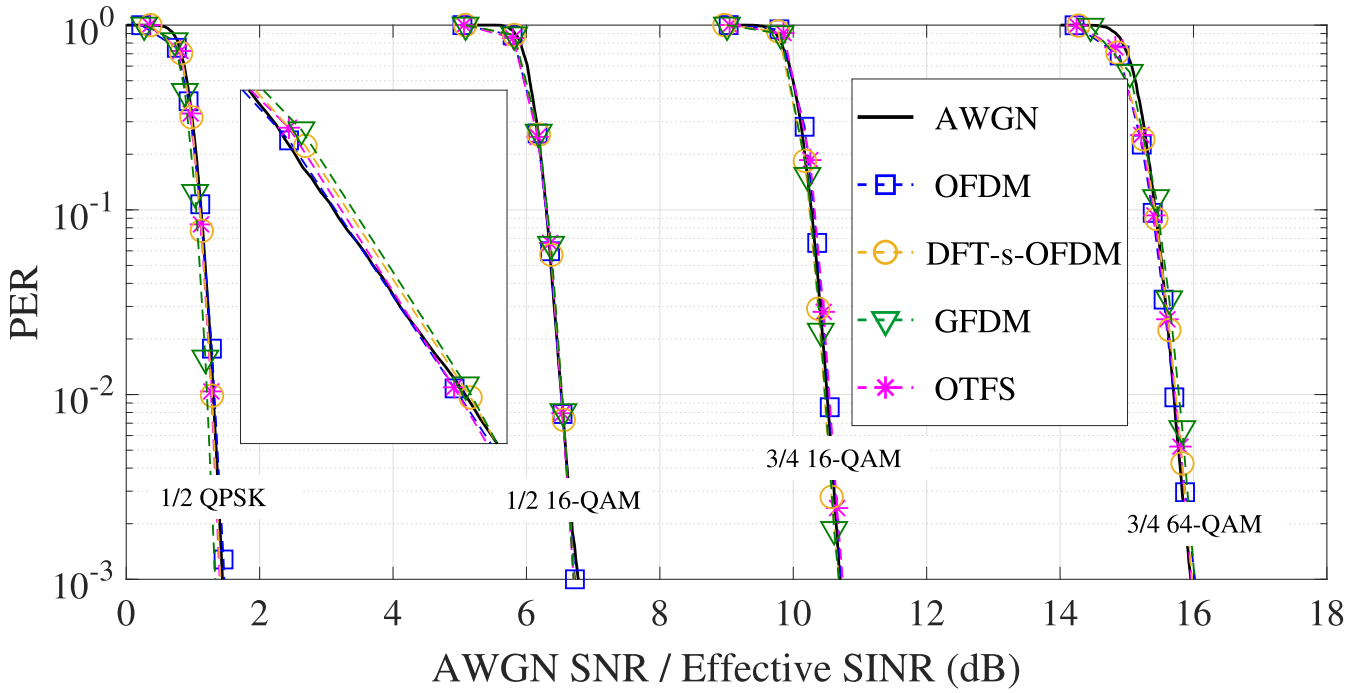

Fig. 5. The PER performance of multicarrier techniques in terms of effective SINR.

A. Accuracy of Effective SINR Mapping

The purpose of this investigation is to validate the accuracy of PLA against AWGN curves. The effective SINR vs. PER in a fading channel is obtained using simulations and compared with AWGN reference curves. In the case of a significant mapping error, optimization of β should be carried out for each MCS such that the error between both SINRs (i.e., AWGN and effective SINR for the same value of PER) could be minimized. In Fig. 5, the PER of different MCSs is plotted in AWGN channel, represented with solid lines. Moreover, the effective SINR vs. PER performance in FSF channel is also plotted for multicarrier modulations, represented by markers. It is important to mention that these results are obtained with optimized values of β listed in Table II. The results show perfect overlapping between PER of different multicarrier techniques obtained in a fading channel and PER in the AWGN channel. As explained in the previous section that ideally, the performance of a fading channel as a function of effective

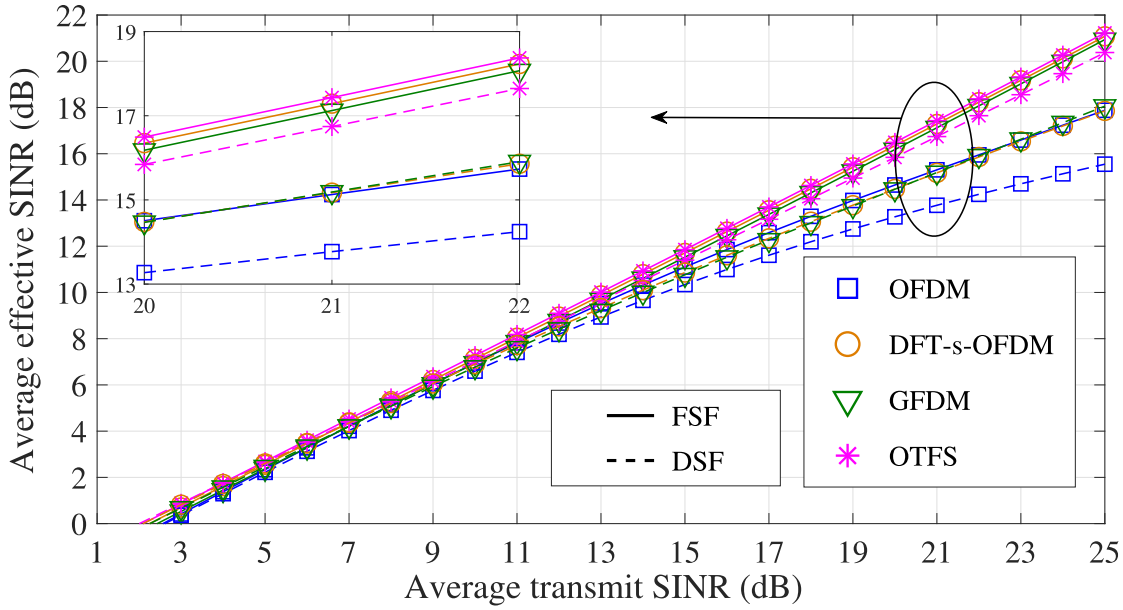

Fig. 6. Effective SINR of various multicarrier modulations under fading conditions (1/2 16QAM).

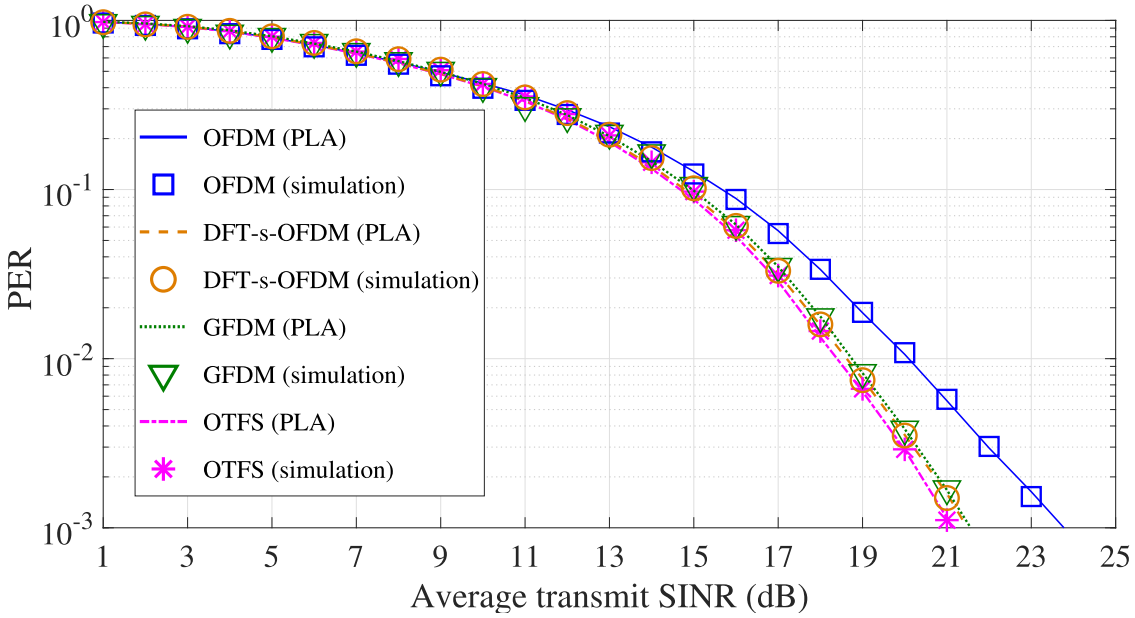

Fig. 7. Estimated and simulated PER of multicarrier modulation techniques under DSF channel.

SINR should have a similar performance as in the AWGN channel. If this holds, a single lookup table per MCS could be used to predict the performance of various multicarrier techniques in a range of fading scenarios. This simplifies system-level simulation as well as link adaptation.

The overlapping PER curves of multicarrier modulations in Fig. 5 do not mean that all modulation techniques have similar performance as a function of transmitted SINR. The transmitted SINR here (γ_{tx} in Fig. 4) means that signal is transmitted with a defined transmit power and interference-plus-noise ratio. In practice various techniques may have different effective SINR, even though, the transmitted SINR is equal. This is shown in Fig. 6, where average effective SINR vs. transmitted SINR of different multicarrier techniques is plotted for FSF and DSF channels with 1/2 16-QAM. Results show that the OTFS outperforms other techniques in terms of effective SINR due to the spreading of signals in both time and frequency domains. Moreover, its effective SINR is least dependent on the channel response. In the case of FSF channel, DFT-s-OFDM and GFDM have comparable performance to OTFS due to similar diversity gain. By contrast, effective SINR difference increases in DSF channel, because OTFS has additional diversity gain due to time selectivity. Comparing DFT-s-OFDM and GFDM, it can be noticed that

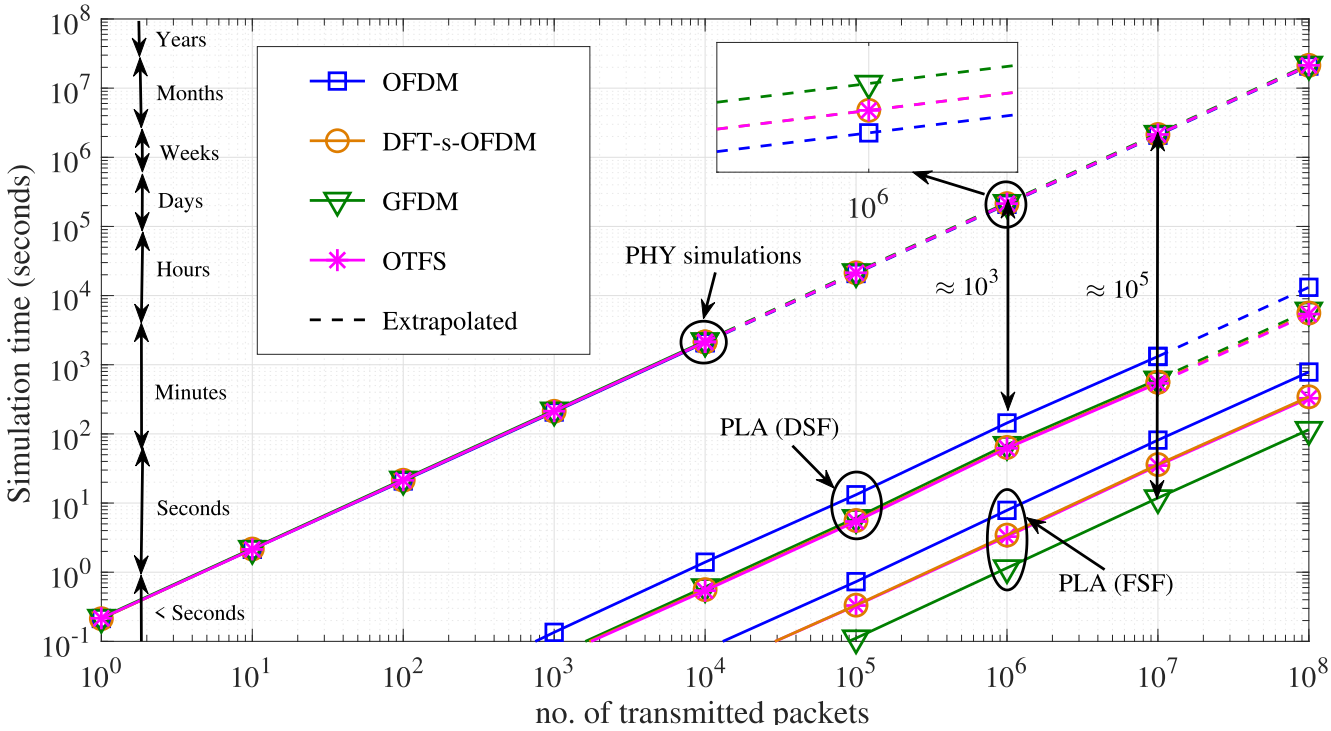

Fig. 8. Comparison between PHY simulation and PLA in terms of simulation time (1/2 16-QAM).

the effective SINR of DFT-s-OFDM is slightly higher for the case of FSF channel and marginally lower for the case of DSF channel (i.e., when transmitting SINR $>$ 20 dB). The better performance of DFT-s-OFDM is due to higher diversity gain from interleaved subcarriers with 4 times lower subcarrier spacing compared to GFDM. In the presence of Doppler lower subscriber spacing result in higher ICI which degrades its performance, as could be observed in the case of DSF channel. Nevertheless, OFDM gives the least amount of effective SINR compared to other multicarrier techniques, and the difference increases with the channel selectivity. The reason is the independent fading experienced by received data symbols with OFDM which results in lower effective SINR due to deep fades. Conversely, in the case of other modulations, deep nulls are averaged out due to the spreading of data in either frequency domain (such as DFT-s-OFDM and GFDM) or in both time and frequency domain (such as OTFS).

B. Prediction Accuracy of PLA

The previous subsection shows that the performance of all multicarrier techniques at a certain effective SINR is equivalent to AWGN SNR. Consequently, lookup tables generated under the AWGN assumption can be used for performance estimation in fading channels. To demonstrate this, PER performance of multicarrier modulations is estimated in a DSF channel. The predicted and simulated PER values are plotted in Fig. 7 for comparison. Once again results demonstrate a good match between predicted and simulated performance for all considered multicarrier techniques. By comparing the performance among multicarrier modulations, a similar trend to Fig. 6 can be observed. An important point to be noted is that Fig. 6 and Fig. 7 show different comparison. The Fig. 6 depict gain in terms of average effective SINR, whereas Fig. 7 compare average PER estimated based on the instantaneous effective SINR. Due to the fact that both gains are not interchangeable, the difference in terms of transmitted SINR is not equal. Furthermore, it is also worth mentioning that the real performance gain of OTFS, DFTs-OFDM, and GFDM can only be achieved through an iterative interference cancellation scheme, which cancels out the ISI among data symbols introduced by MMSE receiver.

C. Simulation Complexity Analysis

In order to give an insight into the reduction in computational complexity by using PLA instead of PHY simulations, a comparison is provided in Fig. 8. The computation time of PHY simulations is almost the same for different multicarrier techniques because they go through similar processing except for additional precoding required in the case of DFT-s-OFDM, GFDM, and OTFS. Therefore, OFDM achieves the lowest simulation time followed by OTFS and DFT-s-OFDM due to DFT and SSFT precoding, respectively. The GFDM requires the highest simulation time due to DFT processing with circular pulse shaping. However, the simulation time of OTFS, GFDM, and DFT-s-OFDM will further increase, if the iterative receiver will be used. Now comparing the computation time of multicarrier techniques when PLA is used, the opposite trend is observed compared to PHY simulation. First considering the DSF channel, PLA of OFDM requires mapping in both time and frequency domain, therefore OFDM requires more computation time. Comparatively, DFT-s-OFDM and GFDM

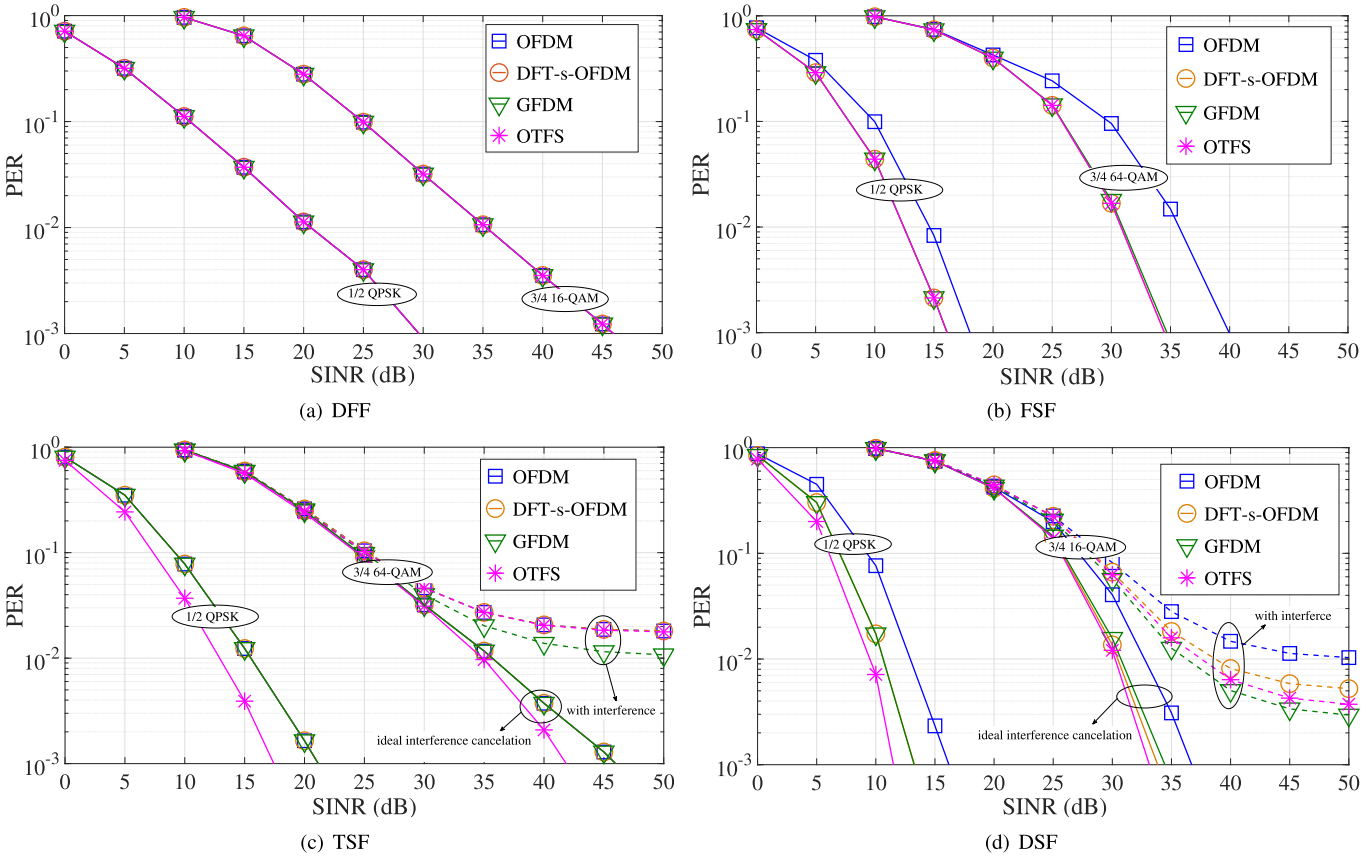

Fig. 9. Performance comparison of multicarrier modulation techniques.

require mapping in the time domain only, and OTFS does not require mapping at all. Even though effective SINR computation is not needed in the case of OTFS, it still needs to calculate the received SINR from $M \times N$ channel matrix. Further, looking at the FSF channel only OFDM requires effective SINR mapping, whereas other techniques require to compute receive SINR from the frequency domain matrix, which is $1 \times N$ for the case of OTFS and DFT-s-OFDM and $1 \times K$ for GFDM. Finally, comparing the PHY simulation with PLA, simulation time can be reduced by a factor of 10^3 in the worst-case scenario, which is OFDM in the DSF channel, and 10^5 in the best-case scenario, which is GFDM in the FSF channel. Hence, it can be concluded that PLA is an effective method to speed up system-level simulations and evaluate higher-order probabilities within an affordable time.

VII. Comparison of Multicarrier Modulation Techniques

In this section, a comparison of modern multicarrier modulation techniques is provided under various fading conditions. Such comparison is generally required to evaluate the pros and cons of a newly proposed technique in reference to the existing ones. In order to compare the performance of multicarrier techniques, a simple system-level simulator is considered with one transmitter and receiver. The concept of link-level to the system-level interface is illustrated in Fig. 4. At the system-level, the arbitrary frequency response of the channel is generated depending on the PDP or fading conditions. The PDP and Doppler shift values for the considered fading conditions (i.e., DFF, TSF, FSF, and DSF) are provided in Table III. The carrier spacing for all multicarrier techniques is equal except for GFDM (M times higher, where M is the number of subsymbols in the GFDM block). For comparison, a lower-order MCS and a higher-order MCS, i.e., 1/2 QPSK and 3/4 64 QAM, are considered. In the case of time selective channels, performance is evaluated considering interference as well as assuming an ideal interference cancellation scheme.

A. Doubly Flat Fading (DFF)

In the case of DFF, the channel is assumed flat in both time and frequency. This type of fading is commonly experienced in indoor environments, having strong LOS components, few weak multipath components, smaller excess delay, and relatively static or slower user speed. Consequently, the choice of carrier spacing and ICI is not relevant ($\tau_s \approx 0$). The channel gain, in this case, could be represented by $\mathbf{H}$ having a single entry. The PER of various multicarrier techniques is shown in Fig. 9(a) for the DFF channel. As packets encounter similar fading conditions irrespective of the used multicarrier technique, all have equal PER. Therefore, the choice of a multicarrier technique does not impact PER performance.

B. Frequency Selective Fading (FSF)

For the case of FSF, the channel is assumed flat in time but selective in frequency. The FSF is encountered in large indoor halls or in outdoor environments, having strong multipath components, large excess delay, and relatively static or slower user speed. Similar to DFF, ICI is not relevant ($\tau_s \approx 0$). However, an ideal interference cancellation scheme is assumed for self-interference due to MMSE equalization. The channel gain for this case is represented by $\mathbf{H}$ having $1 \times N$ entries, where N is the number of subcarriers. The received SINR per block could be obtained using the SINR expressions followed by effective SINR mapping. The PER of considered multicarrier schemes is shown in Fig. 9(b) for the FSF channel. Both OTFS and DFT-s-OFDM deliver almost similar PER performance because they spread symbols in the frequency domain and therefore achieve higher energy per bit compared to OFDM. The GFDM also spread data symbols in the frequency domain, however, with four times less number of subcarriers. Furthermore, the difference in performance among multicarrier techniques is higher for the case of 3/4 64-QAM compared to 1/2 QPSK. This is due to the fact that with the increase in modulation order more bits are transmitted in one OFDM symbol. As a result, more number of bits experience frequency diversity. Furthermore, the performance of all multicarrier techniques is relatively better compared to the DFF channel.

C. Time Selective Fading (TSF)

If the channel response is flat in frequency but selective in time, it is defined here as TSF channel. In Section III, time selectivity is defined by τ_s, its value close to 1 denote highly selective channel and its value close to 0 represent flat channel. Alternatively, a ratio between coherence time and packet duration could also be used. The TSF channel is usually experienced in outdoor environments, having LOS communication, fewer weak multipath components, smaller excess delays, and users moving at high speed. For the used carrier spacing (i.e., 156.25 kHz), the ICI power is only dominated for SINR higher than $30\mathrm{dB}$ (Table I, Fig. 2). Therefore, comparison with and without interference cancellation is only shown for 3/4 64-QAM, as it has a negligible effect on the 1/2 QPSK performance. The TSF channel could be abstracted with $\mathbf{H}$ having $1 \times P$ entries, where P is the total number of blocks in time such that channel in each block could be assumed flat. The received SINR per block could be obtained using the SINR expressions followed by effective SINR mapping. Results for this case are plotted in Fig. 9(c). For the ideal interference cancellation case, it could be observed that all techniques have almost similar performance except OTFS. This is due to the spread of symbol energy over the packet duration in the case of OTFS, which results in higher receive energy per symbol in TSF. Comparing the gain of OTFS between MCSs, 1/2 QPSK has a slightly higher gain compared to 3/4 64-QAM due to the longer packet duration. In the presence of ICI, OTFS performs marginally better compared to OFDM and DFT-s-OFDM, as performance is now ICI dominated. Interestingly, due to higher carrier spacing in GFDM, it outperforms all other multicarrier techniques as it results in lower ICI. Similar to the case of FSF, all multicarrier techniques perform considerably better as compared to the DFF channel. This gain is due to time diversity given that ICI could be ideally equalized. It must be noted that for practical systems, channel estimation error increases with the decrease in coherence time, which results in performance degradation instead of diversity gain. As ideal channel estimation is assumed here, these effects could not be observed from the results.

D. Doubly Selective Fading (DSF)

In DSF, the channel changes rapidly in both time and frequency. Such fading conditions are observed in outdoor environments, having strong multipath components, large multipath excess delays, and users moving at high speed. The eV2X communication scenarios fall generally in this category, such as Urban Crossing NLOS, Highway LOS, and Highway NLOS [18]. Similar to TSF, ICI impacts link performance and needs to be considered. To abstract the DSF channel, $\mathbf{H}$ with $P \times N$ entries is required. The received SINR of each subcarrier in a block could be obtained using the SINR expressions followed by two-fold effective SINR mapping (one in frequency and the other in time domain). The PER performance of multicarrier techniques is depicted in Fig. 9(d). In the case of ideal interference cancellation, OTFS has superior performance compared to other multicarrier techniques. This is due to the spread of symbols in both time and frequency domains which results in higher diversity gain compared to other techniques. Similar to TSF, OTFS gain is slightly higher for 1/2 QPSK compared to 3/4 64-QAM due to longer packet duration. The performance of DFT-s-OFDM is slightly lower than OTFS as it only spread symbols in the frequency domain. The GFDM has a slightly lower gain compared to DFT-s-OFDM due to 4 times less number of subcarriers. The worst performing multicarrier technique is OFDM due to variable SINR per each data symbol. In the presence of ICI, OTFS outperforms OFDM and DFT-s-OFDM due to inherent time and frequency diversity, although GFDM has slightly better performance due to higher carrier spacing. Overall, multicarrier techniques have better performance compared to other fading scenarios if ICI could be equalized. This is due to the higher time and frequency diversity experienced by symbols.

E. Concluding Remarks

The presented comparison can be summarized as:

- In the DFF channel, no gain over a single carrier could be achieved by using any multicarrier technique due to flat fading.
- The PER of all multicarrier techniques decreases with the increase in time-frequency selectivity, given that, the ideal channel estimation and interference cancellation is possible.
- Overall OTFS performs better compared to other multicarrier techniques in all evaluated scenarios, although the gain is higher in the DSF channel.
- In eV2X communication scenarios performance is mainly ICI limited. Consequently, the multicarrier technique with

ICI cancellation scheme performs better, as claimed for OTFS [2].

- Comparing both complexity and performance: OTFS is the best suited for time-varying channels, DFT-s-OFDM for the FSF channel, and GFDM for ICI dominated scenarios.

VIII. Conclusion

In this paper, the modern multicarrier modulation schemes are considered for future wireless communications systems. The received SINR of these multicarrier techniques is derived for the frequency domain MMSE equalization and fading specific PLA is proposed. The accuracy of the proposed PLA is validated through full PHY simulations. Results demonstrate that PLA can precisely estimate PHY performance under various fading conditions. The performance evaluation in terms of effective SINR shows that OTFS delivers higher effective SINR compared to other techniques. The reason for the better performance of OTFS is the spread of symbol energy over time and frequency, which results in higher effective SINR due to higher diversity. Comparison in terms of simulation time shows that PLA for all multicarrier techniques provides a significant gain in terms of simulation time compared to PHY simulations. Multicarrier techniques which spread data symbols in time-frequency have higher gain compared to OFDM, which is due to fewer SINRs required to calculate effective SINR. Overall, a gain of $\approx 10^3$ could be achieved for DSF channel and a gain of 10^5 - 10^6 for FSF channel. The performance comparison among multicarrier techniques shows that in the DFF channel the choice of multicarrier modulation does not affect PER performance. This is due to the fact that all symbols experience similar fading irrespective of the selected technique. Overall, OTFS outperforms all other multicarrier techniques in the DSF channel and has comparable performance to DFT-s-OFDM in the FSF channel. Considering complexity and performance jointly, OTFS is the best-suited multicarrier modulation for time varying channels (such as DSF and TSF), DFT-s-OFDM and GFDM for the FSF channel, and OFDM for DFF channel.

Appendix
Effective SINR Mapping Techniques

A. EESM

The EESM expression is obtained by upper bounding the symbol error probability with Chernoff bound [30]. The generic effective SINR (γ_{eff}) mapping for different modulation schemes can be obtained as [5]

$$\gamma_{\text{eff}} = -\beta \ln\left(\frac{1}{N}\sum_{n=1}^{N}\exp\left(-\frac{\gamma_n}{\beta}\right)\right). \tag{47}$$

The default values of β are the same as in the case of eEESM and can be optimized using (45).

B. RBIR

The effective SINR in the case of RBIR is obtained by first calculating the mutual information per received symbol and then mapping back the mean mutual information to SINR [6]. The effective SINR in the case of RBIR can be calculated as

$$\gamma_{\text{eff}} = \beta\Phi^{-1}\left\{\frac{1}{N}\sum_{n=1}^{N}\Phi\left(\frac{\gamma_n}{\beta}\right)\right\}, \tag{48}$$

where Φ denotes the mean mutual information of the received symbols, given as

$$\Phi(\gamma, M) = \log_2(M) - \frac{1}{M}\sum_{m=1}^{M} E_U\left\{\log_2\left(\sum_{k=1}^{M}\exp\left(|U|^2 - |\sqrt{\gamma}(s_k - s_m) + U|^2\right)\right)\right\}, \tag{49}$$

whereas U is a random Gaussian variable with zero mean and unit variance, E_U represents the expectation of U, s_k denotes the k-th and s_m denote the m-th constellation points, and M represents the total number of bits carried by the used modulation scheme. Similar to EESM, β is the optimization parameter and its default value for all modulation schemes is equal to 1, whereas optimized values are obtained using (45).

C. Enhanced EESM (eEESM)

As mentioned earlier, the eEESM expression is derived by using another tighter bound on SER [11]. The missing derivation steps from Section V are given here.

After applying log and some mathematical manipulations of (43) leads to

$$\log(2\gamma_{\text{eff}} + 1) + 2\gamma_{\text{eff}} = -2\log\left(\frac{1}{N}\sum_{n=1}^{N}\frac{1}{\sqrt{2\gamma_n + 1}}\exp(-\gamma_n)\right). \tag{50}$$

After adding 1 and applying exponent on both side, we get

$$(2\gamma_{\text{eff}} + 1)\exp(2\gamma_{\text{eff}} + 1) = \left(\frac{1}{N}\sum_{n=1}^{N}\frac{1}{\sqrt{2\gamma_n + 1}}\exp(-\gamma_n)\right)^{-2}\exp(1). \tag{51}$$

Now, solving for γ_{eff}, we get

$$\gamma_{\text{eff}} = \frac{1}{2}\left\{\mathcal{W}\left[\exp(1)\left(\frac{1}{N}\sum_{n=1}^{N}\frac{1}{\sqrt{2\gamma_n + 1}}\exp(-\gamma_n)\right)^{-2}\right] - 1\right\}. \tag{52}$$

A generic expression for eEESM is given in (44).

Acknowledgment

The authors alone are responsible for the content of the article.

REFERENCES

[1] W. Anwar, A. Kumar, N. Franchi, and G. Fettweis, "Performance analysis using physical layer abstraction modeling for 5G and beyond waveforms," in *Proc. IEEE Global Commun. Conf. (GLOBECOM)*, Waikoloa, HI, USA, Dec. 2019, pp. 1–6.

[2] T. Zemen, M. Hofer, and D. Loeschenbrand, "Low-complexity equalization for orthogonal time and frequency signaling (OTFS)," *CoRR*, vol. abs/1710.09916, pp. 1–5, Oct. 2017.

[3] R. Hadani *et al.*, "Orthogonal time frequency space modulation," in *Proc. IEEE Wireless Commun. Netw. Conf. (WCNC)*, Mar. 2017, pp. 1–6.

[4] A. C. Mesa *et al.*, "Link abstraction models for multicarrier systems: A logistic regression approach," *Int. J. Commun. Syst.*, vol. 31, no. 1, p. e3436, Sep. 2017.

[5] J. Olmos, A. Serra, S. Ruiz, M. García-Lozano, and D. Gonzalez, "Exponential effective SIR metric for LTE downlink," in *Proc. IEEE 20th Int. Symp. Pers., Indoor Mobile Radio Commun.*, Sep. 2009, pp. 900–904.

[6] R. P. F. Hoefel and O. Bejarano, "On application of PHY layer abstraction techniques for system level simulation and adaptive modulation in IEEE 802.11ac/ax systems," *J. Commun. Inf. Syst.*, vol. 31, no. 1, pp. 198–210, Jan. 2016.

[7] J. Wu, Z. Yin, J. Zhang, and W. Heng, "Physical layer abstraction algorithms research for 802.11n and LTE downlink," in *Proc. Int. Symp. Signals, Syst. Electron.*, Sep. 2010, pp. 1–4.

[8] J. Francis and N. B. Mehta, "EESM-based link adaptation in point-to-point and multi-cell OFDM systems: Modeling and analysis," *IEEE Trans. Wireless Commun.*, vol. 13, no. 1, pp. 407–417, Jan. 2014.

[9] W. Anwar, K. Kulkarni, T. R. Augustin, N. Franchi, and G. Fettweis, "PHY abstraction techniques for IEEE 802.11p and LTE-V2V: Applications and analysis," in *Proc. IEEE Globecom Workshops (GC Wkshps)*, Abu Dhabi, UAE, Dec. 2018, pp. 1–7.

[10] W. Anwar, S. Dev, K. Kulkarni, N. Franchi, and G. Fettweis, "On PHY abstraction modeling for IEEE 802.11ax based multi-connectivity networks," in *Proc. IEEE Wireless Commun. Netw. Conf. (WCNC)*, Apr. 2019, pp. 1–7.

[11] W. Anwar, S. Dev, A. Kumar, N. Franchi, and G. Fettweis, "PHY abstraction techniques for V2X enabling technologies: Modeling and analysis," *IEEE Trans. Veh. Technol.*, vol. 70, no. 2, pp. 1501–1517, Feb. 2021.

[12] W. Anwar, A. Kumar, N. Franchi, and G. Fettweis, "Physical layer abstraction for multi-connectivity communications: Modeling and analysis," *IEEE Trans. Wireless Commun.*, vol. 21, no. 3, pp. 1779–1793, Mar. 2022.

[13] W. Anwar, A. Krause, A. Kumar, N. Franchi, and G. P. Fettweis, "Performance analysis of various waveforms and coding schemes in V2X communication scenarios," in *Proc. IEEE Wireless Commun. Netw. Conf. (WCNC)*, Seoul, South Korea, May 2020, pp. 1–8.

[14] R. Gerzaguet *et al.*, "The 5G candidate waveform race: A comparison of complexity and performance," *EURASIP J. Wireless Commun. Netw.*, vol. 1, p. 13, Jan. 2017.

[15] M. Matthé *et al.*, "Generalized frequency division multiplexing: A flexible multi-carrier waveform for 5G," in *5G Mobile Communications*, W. Xiang, K. Zheng, and X. Shen, Eds. Cham, Switzerland: Springer, 2017, doi: 10.1007/978-3-319-34208-5_9.

[16] R. Hadani and A. Monk, "OTFS: A new generation of modulation addressing the challenges of 5G," *CoRR*, vol. abs/1802.02623, pp. 1–38, Feb. 2018.

[17] W. Anwar, N. Franchi, and G. Fettweis, "Physical layer evaluation of V2X communications technologies: 5G NR-V2X, LTE-V2X, IEEE 802.11bd, and IEEE 802.11p," in *Proc. IEEE 90th Veh. Technol. Conf. (VTC-Fall)*, Honolulu, HI, USA, Sep. 2019, pp. 1–7.

[18] M. Kahn, *V2V Radio Channel Models*, Standard IEEE 802.11-14/0259r0, Feb. 2014.

[19] P. Tan and N. C. Beaulieu, "Reduced ICI in OFDM systems using the 'better than' raised-cosine pulse," *IEEE Commun. Lett.*, vol. 8, no. 3, pp. 135–137, Mar. 2004.

[20] R. Song and S.-H. Leung, "A novel OFDM receiver with second order polynomial Nyquist window function," *IEEE Commun. Lett.*, vol. 9, no. 5, pp. 391–393, May 2005.

[21] H.-A.-M. Mourad, "Reducing ICI in OFDM systems using a proposed pulse shape," *Wireless Pers. Commun.*, vol. 40, no. 1, pp. 41–48, Dec. 2006.

[22] H. F. Arrano and C. A. Azurdia, "ICI reduction in OFDM systems using a new family of Nyquist-I pulses," *IEEE Latin Amer. Trans.*, vol. 13, no. 11, pp. 3556–3561, Nov. 2015.

[23] A. F. Molisch, M. Toeltsch, and S. Vermani, "Iterative methods for cancellation of intercarrier interference in OFDM systems," *IEEE Trans. Veh. Technol.*, vol. 56, no. 4, pp. 2158–2167, Jul. 2007.

[24] W.-S. Hou and B.-S. Chen, "ICI cancellation for OFDM communication systems in time-varying multipath fading channels," *IEEE Trans. Wireless Commun.*, vol. 4, no. 5, pp. 2100–2110, Sep. 2005.

[25] S. Wang, J. S. Thompson, and P. M. Grant, "Closed-form expressions for ICI/ISI in filtered OFDM systems for asynchronous 5G uplink," *IEEE Trans. Commun.*, vol. 65, no. 11, pp. 4886–4898, Nov. 2017.

[26] R. Datta, G. Fettweis, Z. Kollár, and P. Horváth, "FBMC and GFDM interference cancellation schemes for flexible digital radio PHY design," in *Proc. 14th Euromicro Conf. Digit. Syst. Design*, Aug. 2011, pp. 335–339.

[27] S. Aggarwal, "A survey-cum-tutorial on approximations to Gaussian Q function for symbol error probability analysis over Nakagami-m fading channels," *IEEE Commun. Surveys Tuts.*, vol. 21, no. 3, pp. 2195–2223, 3rd Quart., 2019.

[28] J. R. Barry, D. G. Messerschmitt, and E. A. Lee, *Digital Communication*, 3rd ed. Norwell, MA, USA: Kluwer, 2003.

[29] R. M. Corless, G. H. Gonnet, D. E. G. Hare, D. J. Jeffrey, and D. E. Knuth, "On the Lambert-$\mathcal{W}$ function," *Adv. Comput. Math.*, vol. 5, no. 1, pp. 329–359, Dec. 1996.

[30] M. Chiani, D. Dardari, and M. K. Simon, "New exponential bounds and approximations for the computation of error probability in fading channels," *IEEE Trans. Wireless Commun.*, vol. 2, no. 4, pp. 840–845, Jul. 2003.

Waqar Anwar received the bachelor's degree in telecommunication engineering from COMSATS Pakistan, in July 2011, the master's degree in electrical engineering and information technology from the Karlsruhe Institute of Technology, Germany, in September 2014, and the Ph.D. degree in electrical engineering from the Technical University of Dresden, in June 2021. From 2014 to 2016, he was a Research Assistant at Gent University, Belgium. His research at Gent University was focused on throughput optimization techniques in heterogeneous networks. In May 2016, he joined as a Research Associate with the Vodafone Chair of Mobile Communication Systems, Technical University of Dresden, Germany. His current research interests include ultra-reliable communication, multi-connectivity, physical layer abstraction, simulation and evaluation of wireless technologies, and dynamic link adaptation.

Atul Kumar received the B.Tech. degree in electronics and communication engineering in 2013, and the M.S. degree in electronics engineering in September 2015, and the Ph.D. degree in information engineering from the Dipartimento di Elettronica, Informazione, and Bioingegneria, Politecnico di Milano, Milan, Italy, in December 2018. From 2018 to 2021, he was at Gerhard Fettweis' Vodafone Chair, Dresden University of Technology (TU Dresden), where he was a Research Associate. He is currently an Assistant Professor with the Department of Electronics Engineering, IIT (BHU) Varanasi, India. Since 2017, he has been the Director of AtlaMedico TechSolutions Pvt. Ltd., he founded the company for the development of a wireless medical device for intensive care units, India, a technology start-up for the design, optimization, and operation of the medical device. His main research interests include 6G, wireless cellular systems, synchronization errors, joint sensing and communication technology, AI techniques for end-to-end (E2E) prediction of critical quality-of-service (QoS), new radio, massive MIMO (mMIMO), orthogonal frequency division multiplexing, generalized frequency division multiplexing, the Internet of Things, and narrowband power line commutations.

Norman Franchi (Member, IEEE) was born in Hof/Saale, Germany. He received the Dipl.-Ing. (M.S.E.E.) degree in electrical, electronic and communications engineering (EEI) and Dr.-Ing. (Ph.D.E.E.) both from the the Friedrich-Alexander-University (FAU) of Erlangen–Nuremberg, Germany, in 2007 and 2015, respectively. From 2007 to 2011, he was with Continental AG and iSyst Intelligent Systems GmbH, Nuremberg and Regensburg, Germany, where he worked at the Automotive Research and Development Sector as a System and Application Engineer for design and test of advanced networked control systems. From 2012 to 2015, he was at the Institute for Electronics Engineering, FAU, Germany. From 2015 to 2021, he was at the Gerhard Fettweis' Vodafone Chair, Dresden University of Technology (TU Dresden), where he was a Senior Research Group Leader for resilient mobile communications systems and 5G industrial campus networks. From 2019 to 2020, he was the Managing Director of the 5G Lab GmbH, Germany. In 2020, he founded the company Advancing Individual Networks (AIN) GmbH, Germany—a technology start-up for design, optimization, and operation of industrial 5G networks. He is a Full Professor with FAU of Erlangen–Nuremberg, where he has been the Head of the Institute for Electrical Smart City Systems, since 2021. He has been a member of the 5G Lab Germany since 2015. He is an advisory board member of the Industrial Radio Lab Germany (IRLG). His research interests include 6G, 5G, control-communications co-design, resilience in wireless communications systems, joint radio sensing and communications, multi-connectivity in mobile networks, and cognitive radio systems.

Gerhard Fettweis (Fellow, IEEE) received the Ph.D. degree under the supervision of Prof. H. Meyr's from RWTH Aachen in 1990. He was at IBM Research, San Jose, CA, USA, and TCSI Inc., Berkeley, CA, USA. Since 1994, he has been a Vodafone Chair Professor with TU Dresden. He has been the Head of the Barkhausen Institute since 2018. He coordinates the 5G Lab Germany, and has coordinated two German Science Foundation (DFG) Centers at TU Dresden, namely cfaed and HAEC. In Dresden, his team has spun-out seventeen start-ups, and setup funded projects in volume of close to EUR 1/2 billion. In 2019, he was elected into the DFG Senate. His research interests include wireless transmission and chip design for wireless/IoT platforms, with 20 companies from Asia/Europe/U.S. sponsoring his research. He also serves on the board of National Instruments Corp, and advises other companies. He is a Co-Chair of the IEEE 5G/Future Networks Initiative, and has helped organizing IEEE conferences, most notably as a TPC Chair of ICC 2009 and TTM 2012, and as a General Chair of VTC Spring 2013 and DATE 2014. He is a member of the German Academy of Sciences (Leopoldina) and the German Academy of Engineering (acatech). He received multiple IEEE recognitions and has the VDE ring of honor.